Whither BCH2? An ab initio inquiry

Whither BCH_2? An *Ab Initio* Inquiry.

Riccardo Tarroni[1)] and Dennis J. Clouthier[2a)]

[1] *Dipartimento di Chimica Industriale "Toso Montanari", Università di Bologna, Via Piero Gobetti 85, I-40129 Bologna, Italy*

[2]*Ideal Vacuum Products, LLC, 5910 Midway Park Blvd. NE, Albuquerque, New Mexico 87109, USA*

[a)] Author to whom correspondence should be addressed. Electronic mail: djc@idealvac.com

ABSTRACT

The boron methylene (BCH_2) free radical has never been identified spectroscopically. We have undertaken a series of *ab initio* calculations to predict the molecular structures, vibrational frequencies and energies of the ground and first three electronically excited states of BCH_2 and its various isomers and isotopologues. In the ground state, we find that the global minimum is linear HBCH, with C_{2v} BCH_2 some 3 935 cm^{-1} higher and the unstable CBH_2 species is a C_{2v} weakly bound structure at 16 384 cm^{-1} which readily isomerizes to the linear radical. HBCH and BCH_2 are separated by a large isomerization barrier (12 825 cm^{-1}) so it may be possible to prepare boron methylene in the gas phase and detect it with spectroscopic methods. The vibrational frequencies and rotational constants of four ground state isotopologues of BCH_2 have been calculated as an aid to future IR matrix isolation and gas phase microwave studies. Similar calculations are reported for the ground state linear HBCH species and its *cis*- and *trans*-bent excited states. The $\tilde{C}^2B_2$ - $\tilde{X}^2A_1$ electronic transition in the 320 - 290 nm region is the only viable option for detecting BCH_2 by gas phase absorption or laser-induced fluorescence techniques. Franck-Condon simulations of the $\tilde{C} - \tilde{X}$ absorption and the allowed $\tilde{C} - \tilde{X}$ and $\tilde{C} - \tilde{B}$ emission transitions have been done for $^{11}BCH_2$ and $^{11}BCD_2$. In addition, the rotational structure expected for the 0-0 bands of both isotopologues under supersonic expansion conditions has been simulated. The *ab initio* data and predicted spectra should be invaluable for attempts to identify the boron methylene free radial in the gas phase.

I. INTRODUCTION

We have recently reported the $\tilde{B}^2A_2$ - $\tilde{X}^2B_1$ electronic spectra of the jet-cooled aluminum methylene ($AlCH_2$)[1] and gallium methylene ($GaCH_2$)[2] free radicals, along with an extensive *ab initio* study[3] of the ground and electronic excited states of $AlCH_2$. Neither species had previously been observed spectroscopically, either in the gas phase or in matrices, so our work provided the first information on the vibrational frequencies, electronic states, and molecular structures of these novel species. The radicals were produced in an electric discharge jet from a precursor mixture of the vapor of the appropriate metal trimethyl compound [$Al(CH_3)_3$ or $Ga(CH_3)_3$] in high pressure argon and detected by laser-induced fluorescence (LIF) methods. Since trimethylborane [$B(CH_3)_3$] is readily synthesized from the reaction of trimethyl aluminum with boron tribromide,[4] we speculated, perhaps naively, that boron methylene (BCH_2) might also be detectable by LIF spectroscopy. These experiments, conducted both at the University of Kentucky in the years 2015-2017 and at Ideal Vacuum Products in 2019, were an unqualified failure, with no evidence of spectra that could be attributed to the BCH_2 free radical throughout the visible and edge of the ultraviolet (700 – 350 nm).

A thorough literature search turned up only six papers that mention BCH_2 isomers, five theoretical and one infrared matrix isolation study. In the single experimental work, Andrews and co-workers[5] in 1993 reported the results of codeposition of pulsed laser evaporated boron atoms with a mixture of methane/argon onto a 12 K cold window in which they detected the IR spectra of CH_3BH, H_2CBH_2, $H_2C{=}BH$, $HC{\equiv}BH$. and the secondary reaction product H-B=C=B-H. Although the authors concluded that atomic boron is extremely reactive with hydrocarbons, the BCH_2 species was not detected.

In an early theoretical discussion of multiple bonding in simple aluminum species, Cook and Allen[6] showed that although the ground state of $AlCH_2$ has an Al-C single bond, both BCH_2 and $HBCH_2$ have B-C double bonds, due to the better orbital match of the boron 2s and 2p orbitals with those of methylene. In 1998, Fang and Peyerimhoff[7] explicitly studied the mechanism of the insertion of a boron atom into a methane molecule and found that the reaction to form CH_3BH is quite exothermic [52.6 kcal/mol] with a low barrier [20.8 kcal/mol] and that linear HBCH is only formed by 1,1-H_2 elimination from the CH_3BH molecule. A 2008 quantum chemical study of 154 species in the gas-phase chemical vapor deposition (CVD) reactions in preparing boron carbides from BCl_3 –CH_4 –H_2 precurors briefly mentions BCH_2 and HBCH, but they do not appear to be of much importance in the growth processes.[8] More recently, in 2015, Jing *et al*.[9] predicted the properties of larger BCH_x species and identified six novel radicals [CBH_6, C_2BH_6, C_2BH_8, CB_2H, CB_2H_5 and CB_2H_7] which might be detected under suitable circumstances. Finally, in 2019, Mierzwa *et al.*[10] used topological analysis of electron localization functions to predict the existence of exotic species containing boron-carbon double and triple bonds. The present *ab initio* study is aimed at providing some guidance for future spectroscopic studies of BCH_2, as well as an attempt to rationalize the reasons why our previous efforts failed.

II. COMPUTATIONAL METHODS

All *ab initio* calculations were performed using the Molpro[11] quantum chemistry program at the Complete Active Space Self-Consistent Field/Internally Contracted Multireference Configuration Interaction (CASSCF/ICMRCI) level of theory[12-15] with the inexpensive but reliable aug-cc-pVTZ basis.[16] Molecular orbitals were optimized with a state averaged computation of the first four electronic states, using an active space of 9 electrons in 10 valence orbitals. Energies

were then calculated by the ICMRCI method using the same active space as reference. Davidson correction with relaxed reference[17,18] , indicated as +Q, was applied only for the estimation of relative energies of the electronic states on the ground and excited state surfaces. Geometry optimizations and frequency calculations were performed without Davidson correction. Additional computations for the ground states of BCH_2 and HBCH were performed with the aug-cc-pVQZ[16] and aug-cc-pwCVTZ[19] bases, to check the effects of increase of the basis size and the inclusion of core correlation. Some Coupled Cluster computations were performed in the early stages of this work, but the method was abandoned because of its inability to retrieve reliable information on the structures and the vibrational frequencies of the excited states.

The *ab initio* results were used to perform Franck-Condon simulations of the absorption and single vibronic level (SVL) emission spectra of the various free radicals as an aid to their future detection by absorption, laser-induced fluorescence, and/or emission spectroscopy. The simulation program, originally developed by Yang et al.[20] and locally modified for the calculation of SVL emission spectra, requires input of the molecular structures, vibrational frequencies, and mass-weighted Cartesian displacement coordinates from the *ab initio* force fields of the two combining electronic states. Franck-Condon factors are then calculated in the harmonic approximation using the exact recursion relationships of Doktorov et al.[21] taking into account both normal coordinate displacement and Duschinsky rotation effects.

In addition, the absorption contours of the $\tilde{C} - \tilde{X}$ 0-0 bands of the boron methylene free radicals (BCH_2 and BCD_2) were simulated under free jet expansion conditions using the very convenient PGOPHER program.[22,23] The input to the calculations were the equilibrium rotational constants in the combining states and the calculated band origins. Electron spin, nuclear hyperfine, and boron isotope effects were neglected in the simulations of the rotational structure.

III. RESULTS AND DISCUSSION

A. Preliminary considerations

Previous *ab initio* studies of the $AlCH_2$ free radical were confounded by UHF orbital instabilities[3] which gave erratic values for the out-of-plane bending vibrational frequency. Although these problems were initially suspected to be due to core correlation effects,[24] a thorough examination of the issue proved that UHF orbital spatial instabilities were the culprit[3] and that core correlation has a minor effect on the vibrational frequencies. The issue was solved by employing CASSCF/ICMRCI methods within the frozen core approximation,[3] and a similar strategy has been employed in the present work.

The ground state vibrations of the molecules studied are numbered using the Herzberg convention in which the vibrations are classified according to their molecular point group symmetry label and sequentially enumerated from high to low frequency. For planar BCH_2 of C_{2v} symmetry these are ν_1 (a_1) = CH_2 symmetric stretch, ν_2 (a_1) = CB stretch, ν_3 (a_1) = CH_2 symmetric bend or scissoring, ν_4 (b_1) = out-of-plane bend, ν_5 (b_2) = antisymmetric CH_2 stretch and ν_6 (b_2) = CH_2 antisymmetric bend or rocking. For consistency, the excited state vibrations and those of BCD_2 are numbered in the same fashion, regardless of their relative numerical values. For HBCH, the vibrations are $\nu_1(\sigma^+)$ CH stretch, $\nu_2(\sigma^+)$ BH stretch, $\nu_3(\sigma^+)$ BC stretch, $\nu_4(\pi)$ bend (boat) and $\nu_5(\pi)$ bend (chair).

Our study started with a survey of the energy profiles of the ground and the first three doublet electronic states along the BCH_2-HBCH-CBH_2 isomerization path. We followed the migrations of the hydrogens of HBCH, either from boron to carbon to form BCH_2 or from carbon

to boron to form CBH_2 using a system of Jacobi coordinates centered on the middle of the BC bond. The coordinate for the migration of H(B) hydrogen was the angle θ_1 between H(B), the middle of the BC bond, and the B atom. The coordinate for the migration of H(C) hydrogen was the angle θ_2 between H(C), the middle of the BC bond, and the C atom (see Fig. 1). Both angles were changed separately from 0° to 150° with 10° increments. For each angular step, the remaining internal coordinates were optimized to minimize the ground state energy. All atoms were assumed to lie on the same plane, to enable faster computations with structures with at least C_s symmetry. This restriction was released in a later step. The results of these computations are summarized in Fig. 1. It should be pointed out that the stationary points shown by the various surfaces are nearly optimized only for the ground state, because the geometric parameters other than θ_1(or θ_2) have been optimized only for this latter. Those on the excited surfaces require separate optimizations, starting from these approximate ones.

The most interesting points of the various surfaces have been associated with the BCH_2 and HBCH structures and labelled with the corresponding spectroscopic term values. Other relevant points such as transition states and the weakly bound CBH_2 species were labeled with lowercase letters. Each point was further characterized by complete geometry optimization followed by a frequency calculation at the CASSCF/ICMRCI level. For ground state structures, we used the aug-cc-pVTZ, aug-cc-pVQZ and aug-cc-pwCVTZ bases, including core correlation for the latter, while for the excited states we used only the aug-cc-pVTZ basis. The results of these calculations are summarized in Tables I-V

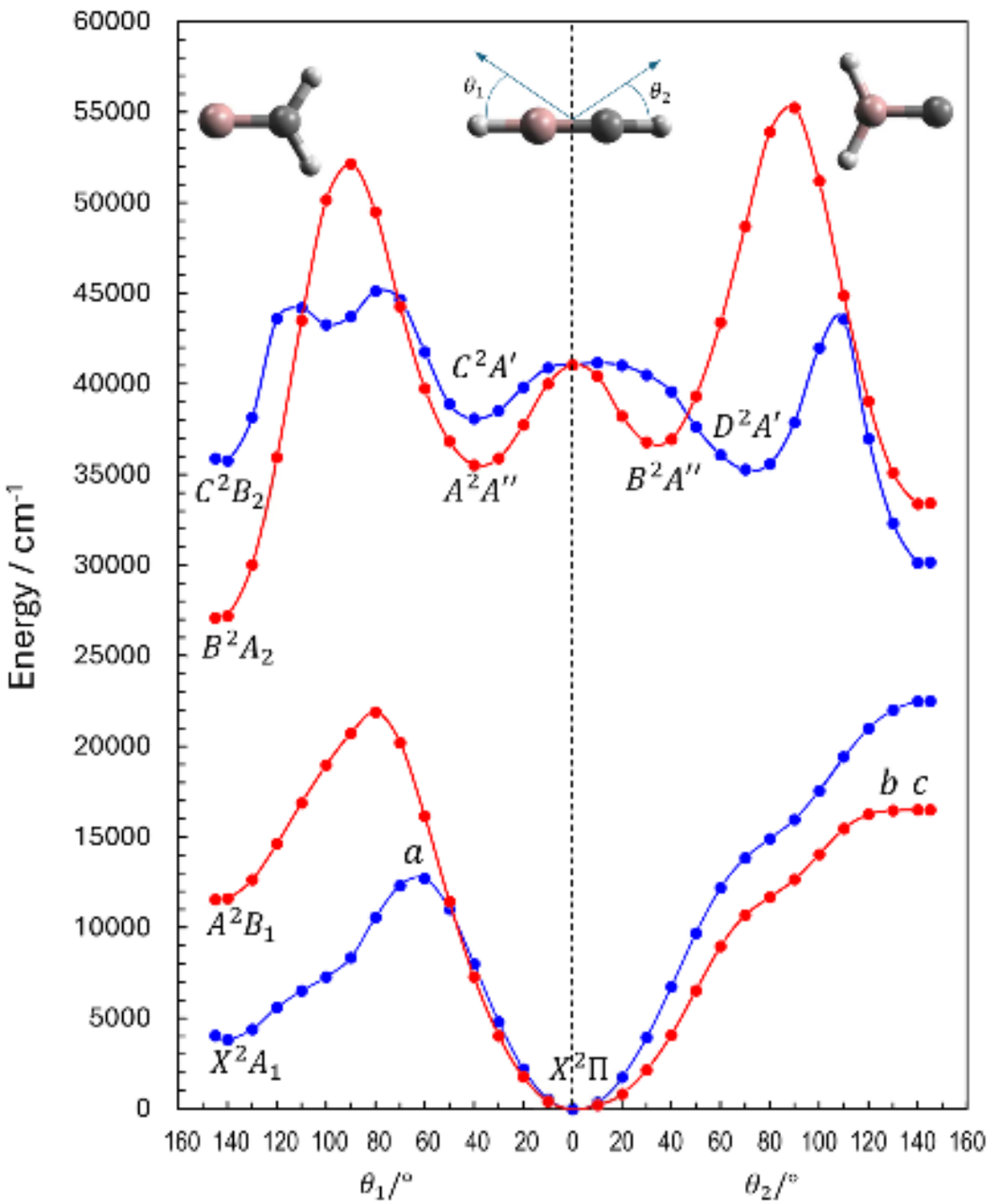

Figure 1: Energy profiles of the lowest electronic states for the B-C-H_2 system, as a function of θ_1 or θ_2 angles. The ground state geometry was optimized with θ_1 and θ_2 alternatively kept fixed. Only planar structures were considered. All computations were performed in C_s symmetry at the ICMRCI/aug-cc-pVTZ level of theory. Blue: A' states. Red: A'' states.

TABLE I. The molecular structures, permanent dipole moments, equilibrium excitation energies and equilibrium rotational constants (MHz) of $^{11}B^{12}CH_2$ and $^{11}B^{12}CD_2$ for the various electronic states.

		$\tilde{X}^2A_1$	$\tilde{A}^2B_1$	$\tilde{B}^2A_2$	$\tilde{C}^2B_2$
r(BC) Å		1.4003	1.5412	1.5329	1.4643
		1.3959[a]	1.5362[a]	1.5278[a]	1.4580[a]
		1.3945[b]	1.5344[b]	1.5266[b]	1.4575[b]
r(CH) Å		1.0859	1.0896	1.0900	1.0849
		1.0847[a]	1.0883[a]	1.0888[a]	1.0838[a]
		1.0841[b]	1.0876[b]	1.0882[b]	1.0831[b]
Θ(HCH) °		117.45	115.06	114.58	124.15
		117.48[a]	115.16[a]	114.58[a]	123.90[a]
		117.42[b]	115.11[b]	114.54[b]	123.83b
Dipole moment (D)[c]		0.119	-2.925	-1.086	0.849
		0.115[a]	-2.950[a]	-1.097[a]	0.883[a]
		0.077[b]	-2.951[b]	-1.104[b]	0.861[b]
T_e (cm^{-1}) [d]		0 (3 935)	4 840	20 332	31 203
		0 (3 996[a])	5 094[a]	20 599[a]	31 337[a]
		0 (4 049[b])	5 125[b]	20 520[b]	31 298[b]
Transition dipole moment (D)[e]	$\tilde{X}^2A_1$		0.690 (x)	-	1.056 (y)
	$\tilde{A}^2B_1$			0.110 (y)	-
	$\tilde{B}^2A_2$				0.876 (x)
A_e (BCH_2) MHz		291 022.7	296 711.7	298 045.1	272 815.6
B_e (BCH_2)		35 895.1	29 940.5	30 202.2	33 662.2
C_e (BCH_2)		31 953.9	27 196.2	27 423.3	29 964.9
A_e (BCD_2) MHz		145 623.2	148 469.9	149 137.1	136 512.6
B_e (BCD_2)		30 674.0	25 740.8	25 933.6	29 189.8
C_e (BCD_2)		25 337.0	21 937.4	22 092.0	24 047.8

[a] aug-cc-pVQZ basis.

[b] aug-cc-pwCVTZ basis, all electrons correlated.

[c] The molecule is oriented with the carbon atom at the origin and boron along the x axis with hydrogens in the yz plane. Positive/negative dipole moments have the positive end on boron/carbons atoms.

[d] Davidson correction applied. The minimum of the $\tilde{X}^2A_1$ state with respect to the $\tilde{X}^2\Pi$ minimum of the linear HBCH structure is given in parentheses.

[e] Evaluated at the $\tilde{X}^2A_1$ geometry with MRCI/cc-pVTZ. The direction of the transition moment is specified in parentheses

TABLE II. The molecular structures, permanent dipole moments, and T_e values for the lowest electronic states of HBCH.

	$\tilde{X}^2\Pi$	$\tilde{A}\,^2A''$ (cis)	$\tilde{C}\,^2A'$ (cis)	$\tilde{B}\,^2A''$ (trans)	$\tilde{D}\,^2A'$ (trans)
r(BC) Å	1.3627	1.5305	1.5208	1.5443	1.6348
	1.3691[a]				
	1.3576[b]				
r(CH) Å	1.0701	1.0901	1.0904	1.0835	1.1044
	1.0686[a]				
	1.0684[b]				
r(BH) Å	1.1717	1.1973	1.2027	1.1877	1.1910
	1.1702[a]				
	1.1696[b]				
θ(BCH) °	-	136.77	138.78	141.08	110.87
θ(CBH) °	-	122.62	119.16	125.62	123.78
ϕ (HBCH) °	-	0	0	180	180 [c]
Dipole moment (D)	0.033	1.403	0.409	1.183	0.703
	0.035[a]				
	0.064[b]				
T_e (cm^{-1}) [d]	0	28 625	31 309	30 433	31 482

[a] aug-cc-pVQZ basis

[b] aug-cc-pwCVTZ basis, all electrons correlated

[c] The structure of this state is not truly planar, since the torsion mode has an imaginary frequency (see Table IV)

[d] Davidson correction applied

Table III. The calculated ground and excited state vibrational frequencies (CCSD/aug-cc-pVTZ IR intensities km/mol in parentheses) for the various isotopologues of BCH_2.

Vibration	$^{11}BCH_2$	$^{10}BCH_2$	$^{11}BCD_2$	$^{10}BCD_2$
$\tilde{X}^2A_1$				
$\nu_1(a_1)$ CH_2 sym str	3125.8(8)	3125.9(8)	2276.7(9)	2277.5(9)
	3129.3[a]	3129.4[a]	2279.5[a]	2280.2[a]
	3134.3[b]	3134.4[b]	2283.1[b]	2284.0[b]
$\nu_2(a_1)$ BC str	1444.2(32)	1473.0(31)	1399.6(21)	1434.1(22)
	1453.3[a]	1482.8[a]	1409.5[a]	1444.3[a]
	1455.4[b]	1484.6[b]	1410.6[b]	1445.3[b]
$\nu_3(a_1)$ CH_2 sym bend	1261.0(2)	1270.3(3)	929.1(4)	932.9(4)
	1262.2[a]	1271.1[a]	929.2[a]	932.9[a]
	1266.5[b]	1275.7[b]	933.0[b]	936.8[b]
$\nu_4(b_1)$ o-o-p bend	546.1(29)	546.7(29)	434.4(18)	435.1(18)
	565.6[a]	566.2[a]	449.9[a]	450.7[a]
	566.0[b]	566.6[b]	450.2[b]	451.0[b]
$\nu_5(b_2)$ antisym CH_2 str	3213.3(2)	3213.4(2)	2384.8(1)	2384.8(1)
	3219.6[a]	3219.6[a]	2389.2[a]	2389.3[a]
	3224.3[b]	3224.3[b]	2392.7[b]	2392.8[b]
$\nu_6(b_2)$ antisym CH_2 bend	493.3(1)	495.3(1)	388.2(1)	390.7(1)
	491.2[a]	493.2[a]	386.7[a]	389.2[a]
	494.1[b]	496.1[b]	388.9[b]	391.5[b]
$\tilde{A}^2B_1$				
$\nu_1(a_1)$ CH_2 sym str	3088.2	3088.2	2242.9	2243.1
$\nu_2(a_1)$ BC str	1022.4	1049.1	1149.9	1164.7
$\nu_3(a_1)$ CH_2 sym bend	1401.6	1403.4	892.4	906.6
$\nu_4(b_1)$ o-o-p bend	1134.7	1135.8	899.8	901.2
$\nu_5(b_2)$ antisym CH_2 str	3182.9	3182.9	2363.1	2363.1
$\nu_6(b_2)$ antisym CH_2 bend	542.2	544.0	422.8	425.2
T_0 (cm^{-1}) [c]	4 984	4 979	4 919	4 914
$\tilde{B}^2A_2$				
$\nu_1(a_1)$ CH_2 sym str	3055.1	3055.1	2210.8	2210.9
$\nu_2(a_1)$ BC str	1100.8	1131.1	1144.2	1161.1
$\nu_3(a_1)$ CH_2 sym bend	1444.0	1444.0	998.5	1012.5
$\nu_4(b_1)$ o-o-p bend	579.7	580.3	460.0	460.8
$\nu_5(b_2)$ antisym CH_2 str	3129.8	3129.8	2327.7	2327.7
$\nu_6(b_2)$ antisym CH_2 bend	907.9	911.1	707.4	711.4
T_0 (cm^{-1}) [c]	20 399	20 395	20 350	20 347
$\tilde{C}^2B_2$				

$\nu_1(a_1)$ CH_2 sym str	3078.1	3078.1	2214.5	2214.6
$\nu_2(a_1)$ BC str	1153.2	1179.2	1147.3	1179.1
$\nu_3(a_1)$ CH_2 sym bend	1279.0	1285.1	929.3	930.5
$\nu_4(b_1)$ o-o-p bend	803.5	804.1	634.4	635.3
$\nu_5(b_2)$ antisym CH_2 str	3214.2	3214.2	2403.2	2403.2
$\nu_6(b_2)$ antisym CH_2 bend	953.7	957.3	740.5	745.2
T_0 (cm^{-1}) [c]	31 402	31 399	31 331	31 329

[a] aug-cc-pVQZ basis

[b] aug-cc-pwCVTZ basis, all electrons correlated

[c] Davidson correction applied

TABLE IV. The ground and excited state harmonic vibrational frequencies in cm^{-1} (CCSD/aug-cc-pVTZ IR intensities km/mol in parentheses) of the various isotopologues of the HBCH radical. Experimental matrix IR absorption frequencies[5] are given in square brackets.

Vibration	$H^{11}BCH$	$H^{10}BCH$	$D^{11}BCD$	$D^{10}BCD$
$\tilde{X}\,^2\Pi$				
$\nu_1(\sigma^+)$ CH str	3368.1 (36)	3368.6 (36)	2530.6 (36)	2535.8 (39)
	3380.4[a]	3380.8[a]	2539.7[a]	2544.9[a]
	3380.1[b]	3380.5[b]	2539.7[b]	2544.9[b]
	[3248.8]	[3249.9]	[2464.3]	[2469.4]
$\nu_2(\sigma^+)$ BH str	2841.3 (11)	2859.0 (12)	2150.3 (9)	2179.2 (9)
	2845.0[a]	2862.8[a]	2154.2[a]	2183.4[a]
	2844.8[b]	2862.5[b]	2153.9[b]	2583.1[b]
	[2743.4]	[2760.2]	[2097.8]	[2125.7]
$\nu_3(\sigma^+)$ BC str	1536.8 (20)	1569.0 (21)	1405.7 (11)	1424.5 (10)
	1544.8[a]	1576.8[a]	1412.0[a]	1430.7[a]
	1546.1[b]	1578.2[b]	1413.2[b]	1431.9[b]
	[1475.3]	[1497.4]		
$\nu_4(\pi)$ bend (boat)	679.3 (23)	683.5 (22)	510.2 (18)	516.2 (18)
	681.2[a]	685.6[a]	513.2[a]	519.6[a]
	679.9[b]	684.2[b]	511.6[b]	517.8[b]
$\nu_5(\pi)$ bend (chair)	448.4 (41)	449.5 (42)	352.1 (31)	353.4 (32)
	464.0[a]	465.1[a]	364.9[a]	366.1[a]
	458.0[b]	459.1[b]	360.0[b]	361.3[b]
$\tilde{A}\,^2A''$ *(cis)*				
$\nu_1(a')$ CH str	3122.5	3122.7	2303.5	2303.9
$\nu_2(a')$ BH str	2596.0	2606.8	1914.8	1930.8
$\nu_3(a')$ BC str	1190.5	1220.9	1160.5	1188.8
$\nu_4(a')$ HBCH bend (L-shape)	906.9	912.8	725.8	732.8
$\nu_5(a')$ HBCH bend (linearization)	706.3	707.0	509.7	510.4
$\nu_6(a'')$ HBCH torsion	831.8	835.7	649.0	654.1
T_0 (cm^{-1}) [c]	28 302	28 297	28 351	28 347
$\tilde{C}\,^2A'$ *(cis)*				
$\nu_1(a')$ CH str	3112.4	3112.5	2295.8	2296.3
$\nu_2(a')$ BH str	2501.3	2511.7	1843.2	1858.1
$\nu_3(a')$ BC str	1240.2	1266.0	1142.1	1173.7
$\nu_4(a')$ HBCH bend (L-shape)	1056.5	1067.3	906.7	912.3
$\nu_5(a')$ HBCH bend (linearization)	486.7	487.4	348.7	349.0
$\nu_6(a'')$ HBCH torsion	375.5	380.0	326.5	331.0
T_0 (cm^{-1}) [c]	30 695	30 690	30 835	30 830
$\tilde{B}\,^2A''$ *(trans)*				

$\nu_1(a')$ CH str	3203.7	3203.8	2363.5	2363.9
$\nu_2(a')$ BH str	2668.4	2680.0	1971.7	1988.7
$\nu_3(a')$ BC str	1119.5	1148.1	1088.7	1115.6
$\nu_5(a')$ HBCH bend (linearization)	912.6	918.5	718.5	725.1
$\nu_4(a')$ HBCH bend (L-shape)	576.7	576.9	423.9	424.4
$\nu_6(a'')$ HBCH torsion	308.3	308.6	228.8	229.2
T_0 (cm^{-1}) [c]	29 828	29 820	29 959	29 953
$\tilde{D}\ ^2A'$ (trans)				
$\nu_1(a')$ CH str	2983.5	2983.5	2191.1	2191.2
$\nu_2(a')$ BH str	2647.7	2659.2	1955.6	1972.2
$\nu_3(a')$ BC str	997.3	1003.4	908.7	931.6
$\nu_4(a')$ HBCH bend (L-shape)	930.4	954.5	774.2	780.9
$\nu_5(a')$ HBCH bend (linearization)	753.4	754.0	557.8	558.9
$\nu_6(a'')$ HBCH torsion [d]	990.5*i*	993.5*i*	730.3*i*	734.3*i*
T_0 (cm^{-1}) [c]	30 638	30 628	30 770	30 760

[a] aug-cc-pVQZ basis

[b] aug-cc-pwCVTZ basis, all electrons correlated

[c] Davidson correction applied

[d] The frequency of this mode is imaginary, indicating that the geometry of the electronic state is not planar

TABLE V. Structures, relative energies and vibrational frequencies of *a*, *b* and *c* stationary points on the lowest potential energy surface of the B-C-H_2, system (see Figure 1). Structures *a* and *b* are transition states, while *c* (H_2BC) is a weakly bound species. All frequencies are for the ^{11}B-^{12}C-H_2 isotopologue and are listed in decreasing order regardless of their symmetry.

	a	*b*	*c*
Structure symmetry	C_1	C_s	C_{2v}
r(BC) Å	1.3543	1.4892	1.4993
r(CH) Å	1.0749	2.1112	-
r(BH) Å	1.2320	1.1833	1.1937
θ(BCH) °	168.0	34.2	-
θ(CBH) °	87.3	134.2	119.9
ϕ (HBCH) °	5.9	180	-
T_e (cm^{-1})[a]	12 825	16 482	16 384
CH str	3384.0		
BH str	2469.0		
BC str	1569.5		
BCH bend	1109.3		
HBCH torsion	535.0		
CBH bend	875.4*i*		
Asymm. BH str		2732.8	
Symm. BH str		2485.6	
BC stretch		1226.6	
Symm CBH bend		963.5	
Out-of-plane bend		694.5	
Asymm. CBH bend		258.3*i*	
Symm. BH str			2466.3
Asymm. BH str			1270.6
BC str			1156.2
Symm CBH bend			885.7
Asymm. CBH bend			769.1
Out-of-plane bend			740.2

[a] Referred to the equilibrium energy of HBCH, Davidson correction applied.

B. The Electronic Ground State

As we pointed out in the Introduction, the main goal of the present work is to provide effective and reliable information to aid in the experimental detection of the elusive BCH_2 radical. To this end, we also explored the behavior of its dissociation curves along the BC stretch coordinate (Fig. 2) and the orbitals and dominant configurations of the ground and the lowest electronic states (Fig. 3). All calculations were performed in C_{2v} symmetry at the CASSCF/MRCI/aug-cc-pVTZ level of theory. It is apparent that the ground state has A_1 symmetry, whereas the ground states of $AlCH_2$ and $GaCH_2$ have B_1 symmetry and that all BCH_2 states are bound. The CASSCF BCH_2 molecular orbitals, at the equilibrium geometry of the ground state, are illustrated in Fig. 3 along with the dominant electronic configurations and unpaired electron spin densities for the various electronic states.

Ab initio studies have shown[2,3] that the aluminum methylene and gallium methylene C_{2v} structures are the global minima on their respective ground state potential energy surfaces – the corresponding *trans*-bent isomers are ~50 and ~43 kcal/mol higher in energy, respectively. The first major finding of the present work is that the lowest energy B-C-H_2 isomer is actually the linear HBCH species. At the ICMRCI+Q/aug-cc-pVTZ level of theory, BCH_2 is 11.3 kcal/mol (3 935 cm^{-1}) above HBCH and CBH_2 (point *c* in Fig 1) is a weakly bound species at much higher energy, 46.8 kcal/mol (16 383 cm^{-1}) above HBCH.

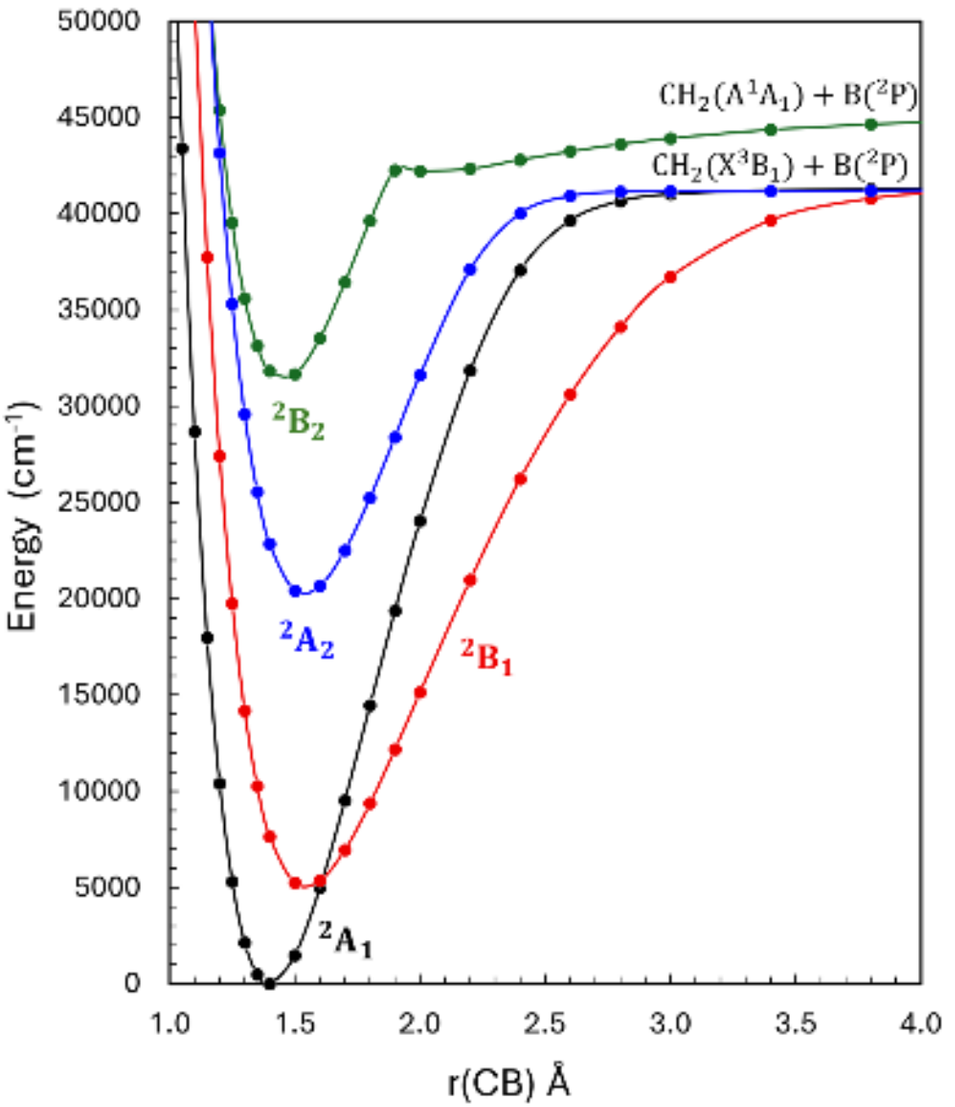

Figure 2: Potential energy curves of the first four electronic states of BCH_2 calculated at the ICMRCI+Q/aug-cc-pVTZ level, as a function of the r(CB) stretching coordinate. The remaining geometric parameters, r_{CH} and θ_{HCH} were fixed at the equilibrium values of the $\tilde{X}^2A_1$ state (see Table I).

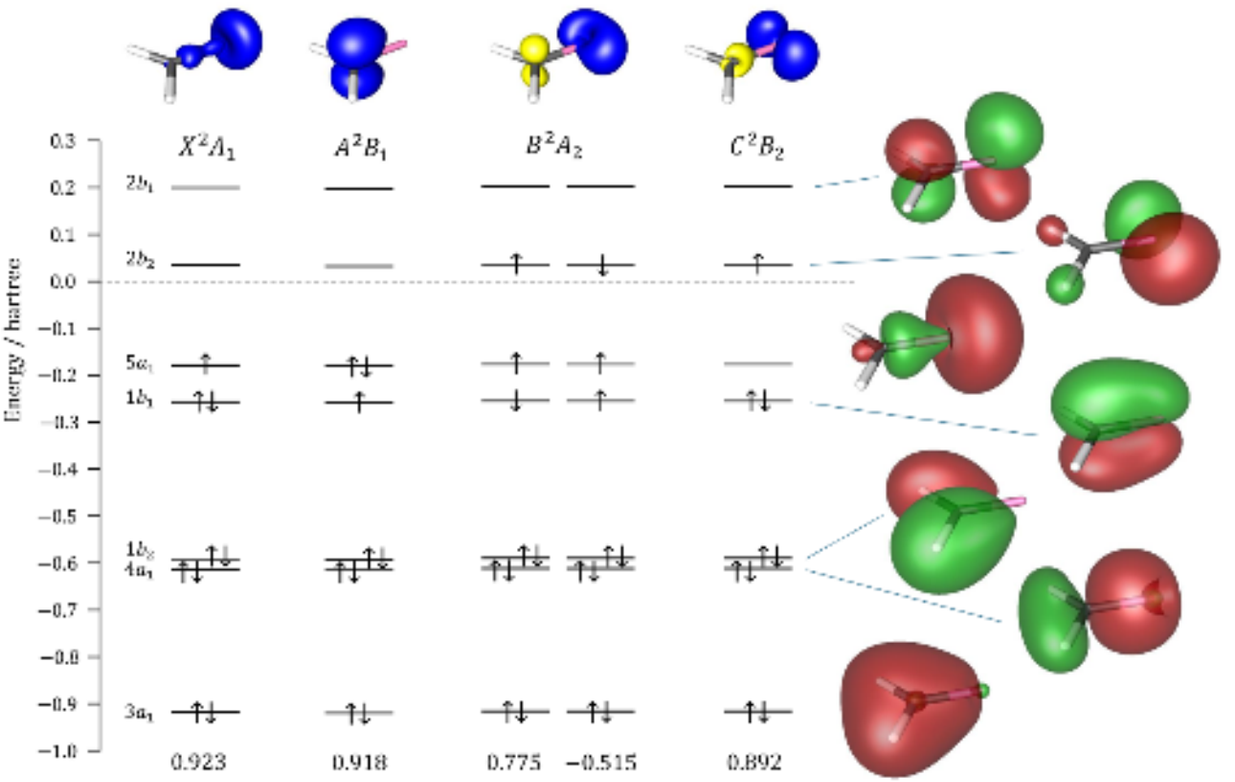

Figure 3. CASSCF/aug-cc-pVTZ valence molecular orbitals, dominant electronic configurations and spin densities for the first four electronic states of BCH_2, calculated at the ICMRCI/aug-cc-pVTZ equilibrium geometry of the ground state. The regions where the difference between α and β spin densities is negative/positive are shown above the MO diagram in light/dark (yellow/blue online).

The isomerization barrier (point *a* in Fig.1) between $B{=}CH_2$ and HBCH is calculated to be 36.7 kcal/mol (12 825 cm^{-1}), so if the experimental synthetic conditions are suitable, it may be possible to produce boron methylene kinetically trapped in its potential well. Such a situation is not unusual. For example, in previous LIF work, we were able to produce H_2PO[25] and H_2PS[26] in electric discharges despite the fact that the *trans*-bent isomers HPOH and HPSH are more stable by ~3 000 and ~1 500 cm^{-1}, (CCSD/aug-c-pVT(+d)Z) respectively. Although HBCH as the global minimum may be the reason that previous IR matrix and gas phase LIF experiments failed to detect the methylenic product, it is entirely possible that different experimental conditions can be found that will produce measurable quantities of $B{=}CH_2$.

The ground state ($\tilde{X}^2A_1$) MO configuration of BCH_2 is:

$$(1a_1)^2\,(2a_1)^2\,(3a_1)^2\,(4a_1)^2\,(1b_2)^2\,(1b_1)^2\,(5a_1)^{\alpha}\,(2b_2)^0$$

and the forms of the frontier molecular orbitals are shown in Fig. 3. The $4a_1$ MO is a σ bonding orbital between boron and carbon, $1b_2$ is essentially an unmodified methylene MO, $1b_1$ is the out-of-plane π bonding orbital, the singly occupied $5a_1$ MO is an *sp* hybrid on B directed away from the CH_2 group and the lowest unoccupied orbital (LUMO b_2) is an in-plane $2p_y$ nonbonding orbital on the boron atom.

The molecular structures, permanent dipole moments and equilibrium rotational constants for the various electronic states of BCH_2 are summarized in Table I with similar information on HBCH collected in Table II. A survey of the literature shows that typical B-C single bond lengths are of the order of 1.54 - 1.61 Å with a representative trimethyl borane [$B(CH_3)_3$] value[27] of 1.578 Å. B-C double-bond lengths from both experimental structures and theoretical calculations fall in the range 1.39-1.44 Å. Early *ab initio* predictions [CISD/TZ2P+] of the BC bond length of the HBCH anion gave a value of 1.323 Å, which was suggested to be the prototypical B≡C bond

length.[28] A more recent calculation [CCSD(T)/aug-cc-pVTZ][10] gave a bond length of 1.339 Å and a topological analysis of the electron localization function (ELF) supported the concept of a B-C triple bond. In contrast, the lowest energy structure of linear HCB is a triplet state[29] with a calculated short bond length of 1.342 Å, which ELF analysis suggests is a carbon-boron double bond.[10] A very recent paper reported the synthesis of a neutral boryne, a stable compound incorporating a boron-carbon triple bond,[30] with a length in the solid state of 1.323 Å. In the present context, the computed (ICMRCI/aug-cc-pVTZ) ground state B-C bond lengths of BCH_2 (1.4003 Å) and HBCH (1.3627 Å) are very similar and precisely as expected for double bonds between boron and carbon.

Cook and Allen[6] discussed the differences and similarities in the bonding of BCH_2 and $AlCH_2$ more than four decades ago. They concluded that BCH_2 should have a B-C double bond and a $^2A_1$ ground state whereas $AlCH_2$ should have an Al-C single bond,[1] now known as an experimental fact, and a $^2B_1$ ground state. The fundamental disparity is that in $AlCH_2$ there are large differences in the orbital energies between aluminum and methylene and the singly occupied HOMO $2b_1$ orbital is essentially an out of plane carbon $2p$ orbital which does not participate in even a partial π bond. In BCH_2, the carbon and boron $2p$ orbitals of similar energy strongly mix, forming a fully occupied π orbital ($1b_1$, Fig. 3) and a double bond with the σ ($4a_1$, Fig. 3) doubly occupied orbital.

The calculated ground state vibrational frequencies and IR intensities of the various isotopologues of BCH_2 and HBCH are summarized in Tables III and IV. BCH_2 is most likely to be detected initially by infrared matrix isolation spectroscopy and the calculations indicate that the most prominent infrared band should be ν_2, the BC stretch in the 1390 – 1475 cm^{-1} region for all 4 isotopologues, with diagnostic isotope shifts. The BC stretches of the corresponding HBCH

species are calculated to be weaker and strongly dependent on the isotopic substitution, with the hydrogenated species about 100 cm^{-1} higher in frequency with respect to the deuterated ones, making them readily distinguishable. The second most intense $^{11}BCH_2$ band is ν_4, the out-of-plane bend at 546 cm^{-1}, whereas the ν_3 fundamental is predicted to be much weaker and at 1260 - 1270 cm^{-1} for BCH_2 and 929 - 933 cm^{-1} for BCD_2, with no HBCH interferences in the same region.

For HBCH the calculated frequencies are always higher by ~100 cm^{-1} with respect to the infrared matrix observations. The agreement is not improved significantly by enlarging the basis size or including core correlation (see Table IV), indicating the presence of substantial matrix effects in the experimental data.

C. The First Excited Electronic State $\tilde{A}^2B_1$

As illustrated in Fig. 2, the first excited state of BCH_2 is the very low-lying $^2B_1$ state, which has a minimum of only 4 840 cm^{-1} above the ground state potential, and electronic configuration

$$(1a_1)^2\,(2a_1)^2\,(3a_1)^2\,(4a_1)^2\,(1b_2)^2\,(1b_1)^{\alpha}\,(5a_1)^2\,(2b_2)^0.$$

The state ordering is just the opposite of that of $AlCH_2$, which has a $^2B_1$ ground state and a nearby $^2A_1$ first excited state, due to the orbital energetic mismatch between Al and CH_2. The BCH_2 excited state predicted geometry and vibrational frequencies are summarized in Tables I and III. The major effects of the electron excitation are a 0.14 Å elongation of the BC bond and a slight closing of the HCH angle (2.4°), reflected in a 309 cm^{-1} decrease in the BC stretching frequency and a 141 cm^{-1} increase in ν_3, the scissoring frequency. The b_1 out-of-plane bending frequency more than doubles in the excited state, from 546 cm^{-1} to 1 135 cm^{-1}.

Although the $\tilde{A} - \tilde{X}$ transition is allowed with a transition dipole moment of 0.69 D, the band system would occur in the near-infrared in a region not amenable to probing by LIF spectroscopy. However, it may be detectable by direct absorption in a matrix, much as the $\tilde{A}\,^2A_2'' - \tilde{X}\,^2A_1'$ transition of B_3 was measured between 6 000 – 8 300 cm^{-1} by Maier and coworkers.[31]

D. The Second Excited Electronic State $\tilde{B}^2A_2$

The dominant electron configurations for the $\tilde{B}^2A_2$ state are

$$(1a_1)^2\,(2a_1)^2\,(3a_1)^2\,(4a_1)^2\,(1b_2)^2\,(1b_1)^{\beta}\,(5a_1)^{\alpha}\,(2b_2)^{\alpha}$$

$$(1a_1)^2\,(2a_1)^2\,(3a_1)^2\,(4a_1)^2\,(1b_2)^2\,(1b_1)^{\alpha}\,(5a_1)^{\alpha}\,(2b_2)^{\beta}$$

in which an electron is promoted from the doubly occupied $1b_1$ (HOMO-1) out-of-plane bonding orbital to the empty $2b_2$ (LUMO) in-plane boron $2p_y$ nonbonding orbital. The promoted electron can be either an α electron or a β electron, so the state cannot be well described by a single configuration. The decrease in bond order results in a 0.13 Å increase in the B−C bond length and a concomitant 3° decrease in the HCH bond angle, almost identical to the deformation in the $\tilde{A}$ state. There is a substantial decrease in the B-C stretching frequency and an almost two-fold increase in the ν_6 (antisymm. CH_2 bend) frequency on electronic excitation. The zero-point energy of the $\tilde{B}$ state of $^{11}BCH_2$ is calculated to be 20 399 cm^{-1} above the zero-point of the ground state but the electronic transition is forbidden by electric dipole selection rules.

E. The Third Excited Electronic State $\tilde{C}^2B_2$

The $\tilde{C}^2B_2$ excited state is formed by promotion of the electron from the $5a_1$ HOMO to the $2b_2$ LUMO (see Fig. 3) and is well described by the single configuration

$$(1a_1)^2\,(2a_1)^2\,(3a_1)^2\,(4a_1)^2\,(1b_2)^2\,(1b_1)^2\,(5a_1)^0(2b_2)^{\,\alpha}$$

The only $^{11}BCH_2$ electric dipole allowed transition within the range of conventional LIF spectroscopy is $\tilde{C}^2B_2$ - $\tilde{X}^2A_1$, whose 0-0 band should occur near 31 315 cm^{-1}. On electronic excitation the BC bond elongates by 0.06 Å and the HCH angle opens by 6.7°, indicating Franck-Condon activity in ν_2' and ν_3' in the absorption and emission spectra, although the ν_2 frequency changes little (1261 → 1279 cm^{-1} for $^{11}BCH_2$) (see Table III). While activity in the nontotally symmetric vibrations is not usually expected in an allowed electronic transition, two quantum transitions such 4_0^2 and 6_0^2 can occur with significant intensity if the vibrational frequencies change substantially on excitation, as they do here (ν_4 = 546 → 804 cm^{-1} and ν_6 = 493 → 954 cm^{-1}).

The top trace in Fig. 4 shows the calculated Franck-Condon profile of the $^{11}BCH_2$ $\tilde{C}$ - $\tilde{X}$ absorption spectrum. The spectrum is dominated by an intense 0-0 band and a short progression in ν_2' along with the anticipated weak activity in ν_3', ν_4' and ν_6'. The $\tilde{C}^2B_2$ state, if emissive, can fluoresce down to the $\tilde{X}$, and $\tilde{B}$ states and the calculated 0^0 level emission spectra are displayed in Fig. 4. Similar results for $^{11}BCD_2$ are shown in Fig. 5.

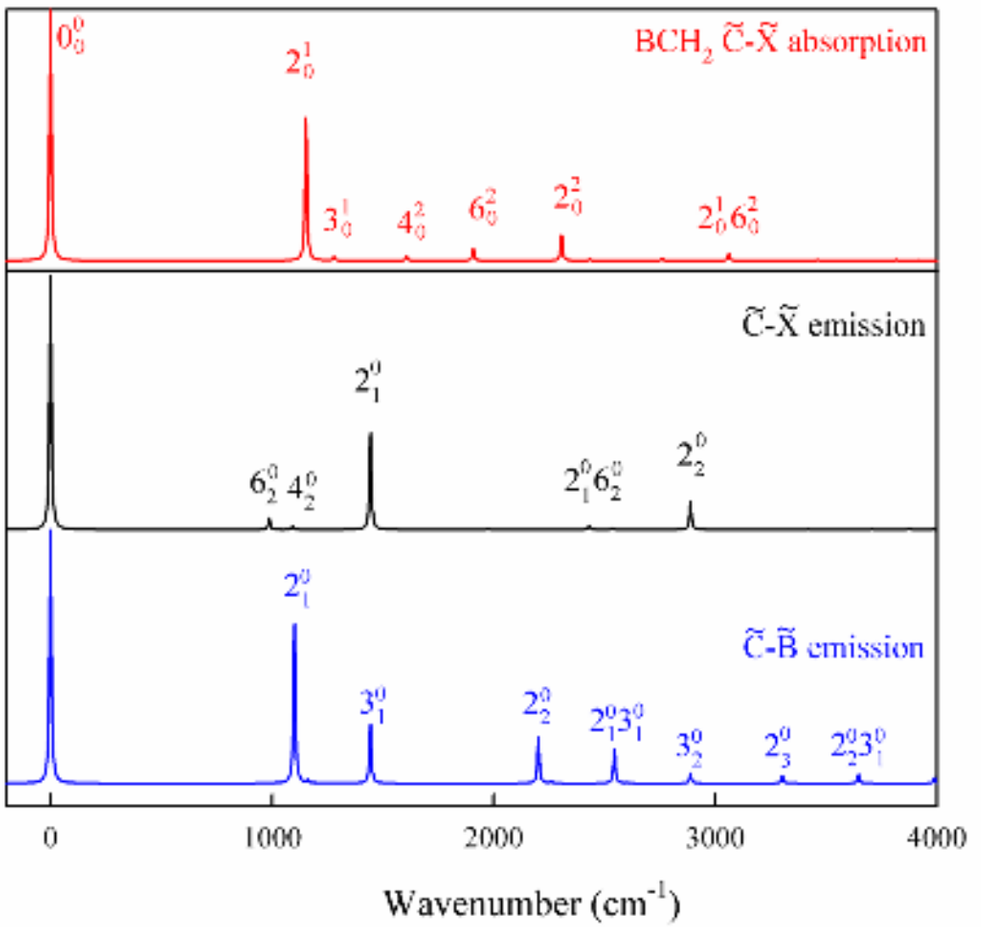

Figure 4: Calculated Franck-Condon profiles of the $\tilde{C}^2B_2$ - $\tilde{X}^2A_1$ absorption spectrum of $^{11}BCH_2$ (top trace) and the emission spectra from the zero-point level of the $\tilde{C}$ state down to the $\tilde{X}^2A_1$ (middle trace) and $\tilde{B}^2A_2$ (bottom trace) electronic states. For the absorption spectrum, the wavenumber scale is cm^{-1} above the 0_0^0 band, estimated at 31 402 cm^{-1}. For the emission spectra, the wavenumber scale is displacement relative to the 0_0^0 bands of the emission transitions which are estimated at $\tilde{C}$- $\tilde{B}$ = 11 003 cm^{-1}.

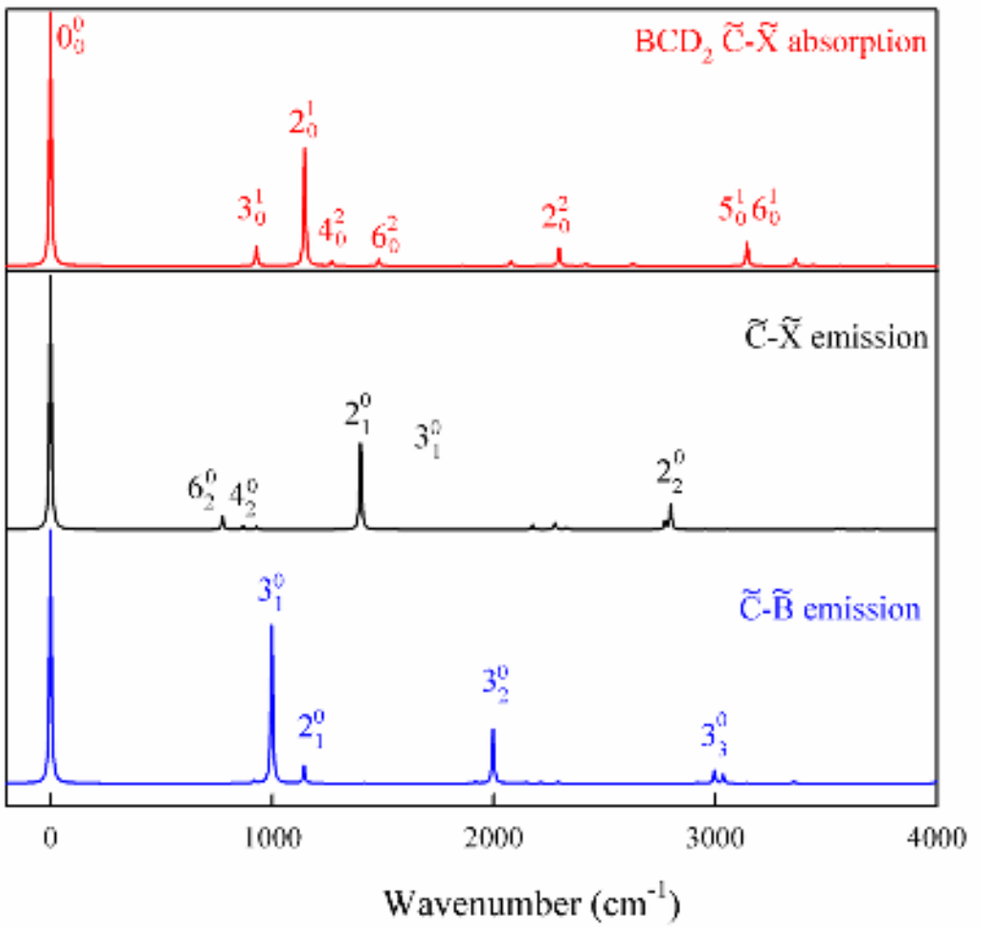

Figure 5: Calculated Franck-Condon profiles of the $\tilde{C}^2B_2$ - $\tilde{X}^2A_1$ absorption spectrum of $^{11}BCD_2$ (top trace) and the emission spectra from the zero-point level of the $\tilde{C}$ state down to the $\tilde{X}^2A_1$ and $\tilde{B}^2A_2$ electronic states. For the absorption spectrum, the wavenumber scale is cm^{-1} above the 0_0^0 band, estimated at 31 331 cm^{-1}. For the emission spectra, the wavenumber scale is displacement relative to the 0_0^0 bands of the emission transitions which are estimated at $\tilde{C}$- $\tilde{B}$ = 10 981 cm^{-1}.

Fig. 6 shows the medium resolution calculated rotational structure of the $\tilde{C}^2B_2$ - $\tilde{X}^2A_1$ 0_0^0 bands of $^{11}BCH_2$ and $^{11}BCD_2$ at a temperature of 20 K with a linewidth of 0.2 cm^{-1}. These are perpendicular bands with the transition moment along the in-plane *b*-axis obeying the selection rules $\Delta K_a = \pm 1$, $\Delta K_c = \pm 1$. Our best *ab initio* estimates for the energies of the 0-0 bands are 31 402 cm^{-1} for $^{11}BCH_2$ and 31 331 cm^{-1} for $^{11}BCD_2$ with calculated ^{11}B – ^{10}B isotopes shifts of 2.1 and 1.8 cm^{-1}, respectively. The BCH_2 nuclear statistical weights favor the odd K_a levels by a factor of 3, so despite the low rotational temperature, the $K_a^{'} = 2$ - $K_a^{''} = 1$ and $K_a^{'} = 0$ - $K_a^{''} = 1$ subbands are stronger than the central $K_a^{'} = 1$ - $K_a^{''} = 0$ subband. In sharp contrast, the BCD_2 nuclear statistical weights are 2:1 for even:odd K_a values, so the central subband is more pronounced than those in the wings. Even at very low resolution, these obvious differences in band shape would be diagnostic for the BCH_2/BCD_2 spectra.

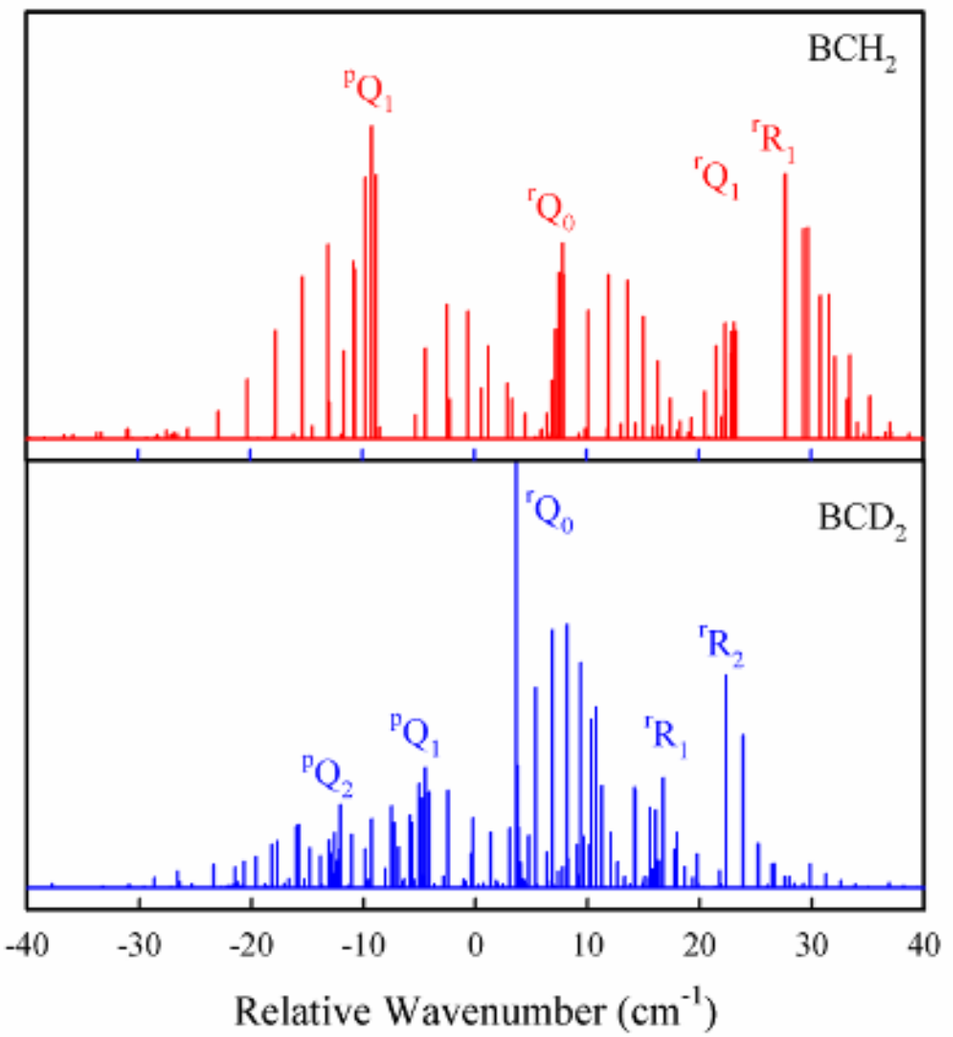

Figure 6: Calculated rotational structure for the $\tilde{C}^2B_2$ - $\tilde{X}^2A_1$ 0_0^0 bands of the boron methylene free radicals at a resolution of 0.2 cm^{-1} and a rotational temperature of 20 K. The equilibrium rotational constants in the combining states were used in the calculations and electron spin, nuclear spin (other than nuclear statistical weights) and boron isotope effects were neglected. The band origins are at 0.0 relative wavenumber and are estimated to occur at $^{11}BCH_2$ = 31 402 cm^{-1} and $^{11}BCD_2$ = 31 331 cm^{-1}.

F. The electronic spectrum of HBCH

Our calculated properties of the HBCH isomer are summarized in Tables II and IV. In the excited state, the linear molecule distorts to a *cis*- or *trans*-bent structure, and the resulting bent-linear transitions would be complex. In addition, the presence of two Renner-Teller active vibrational modes (ν_4 and ν_5) both in the ground and in the excited states greatly complicates the vibronic energy level structure and a complete theoretical description is beyond the scope of this work. Suffice it to say that the presence of HBCH electronic transitions near or at slightly lower energies than those of BCH_2 may muddy the waters in a search for new spectra. Fortunately, BCH_2 and HBCH will have very different vibronic spectra and both are sufficiently light so that the diagnostic rotational structure should be readily resolved, facilitating identification of the carrier of any new spectra that are found.

F. Final Considerations

It is perhaps not too surprising that the lowest energy isomer on the BCH_2 surface is the linear HB=CH structure, whereas $AlCH_2$ and $GaCH_2$ are the global minima on their respective surfaces. The dichotomy between the group III methylenes is reminiscent of similar trends in group IV. Linear acetylene is the global minimum on the C_2H_2 surface, with vinylidene ($C{=}CH_2$) as a higher energy transient isomer. Substitution of a heavier atom (X = Si, Ge, Sn) inverts this state of affairs, with the C_{2v} $X{=}CH_2$ species as the lowest energy isomers.[32-40] In the $AlCH_2$ case, *trans*-HAlCH is a higher energy isomer and the truly linear HCAlH species is a transition state rather than a stable structure.[3] Similarly *trans*-HGaCH ($\tilde{X}^2A''$) is found some 42.8–45.1 kcal/mol higher[2] than $GaCH_2$. With these predictions in mind, we were able to use laser spectroscopic methods to

detect $AlCH_2$ and $GaCH_2$ among the products of an electric discharge through the vapor of trimethyl aluminum and trimethyl gallium, respectively, analogous to our previous studies[32-40] of $SiCH_2$, $GeCH_2$ and $SnCH_2$, produced by discharge degradation of the tetramethyl compounds.

The out-of-plane (oop) bending frequencies (ν_4) of the Group III methylenes also deserve some discussion. A quick perusal of Table VI shows that typical ground state frequencies are of the order of 1000 cm^{-1}, whereas those of BCH_2, $AlCH_2$ and $GaCH_2$ are much lower (546-404 cm^{-1}). It is striking that the atypical frequencies return to "normal" values in the low-lying first excited states, despite the fact that BCH_2 ($\tilde{A}^2B_1$) and $AlCH_2$/$GaCH_2$ ($\tilde{A}^2A_1$) have different $\tilde{A}$ state symmetries and orbital occupations. Reference to the Walsh diagram for H_2AB molecules shows that all the MO's up to and including $2b_2$ (*n* orbital on B atom) increase in energy on out-of-plane (oop) bending, which would resist the oop bending deformation. Reasoning that the Group III anomalous frequencies might be due to the variation of orbital energies on oop bending, we constructed the Walsh-like diagrams shown in Fig. 7. It is our contention that orbitals that decrease in energy on pyramidalization favor lower oop bending frequencies, whereas those that increase in energy favor higher frequencies.

Fig. 7 shows that the two lowest occupied BCH_2 orbitals are $5a_1$ (largely an *sp* hybrid on B) whose energy is invariant to oop deformation and $1b_1$ (a B-C bonding π orbital) which is stabilized by oop bending. At planarity the $1b_1$ (π) orbital consists of contributions from the p_x orbitals on C and B but the lowering of symmetry on bending allows mixing with the *s* orbitals on all centers. According to the Walsh postulate, the greater the *s* orbital character, the greater the stabilization, precisely as observed. The ground state is $\ldots(1b_1)^2\ (5a_1)^1$ and the two electrons in the HOMO-1 π orbital lower the oop bending frequency to 546 cm^{-1}. On promotion of an electron

to form the $\tilde{A}$ state […$(1b_1)^1$ $(5a_1)^2$], the fully occupied b_1 orbital stabilization is reduced yielding $\nu_4' = 1135$ cm^{-1}.

TABLE VI: The ν_4 out-of-plane bending frequencies of various planar methylenic (XCH_2) molecules.

	$\tilde{X}$	$\tilde{A}$	Reference
H_2CO	1167		Expt. ref. 41
H_2CS	990		Expt. ref. 41
H_2CSe	906		Expt. ref. 42
BCH_2	546	1135	Theory-this work
$AlCH_2$	445	1013	Theory-ref. 3
$GaCH_2$	404	981	Theory-ref 2

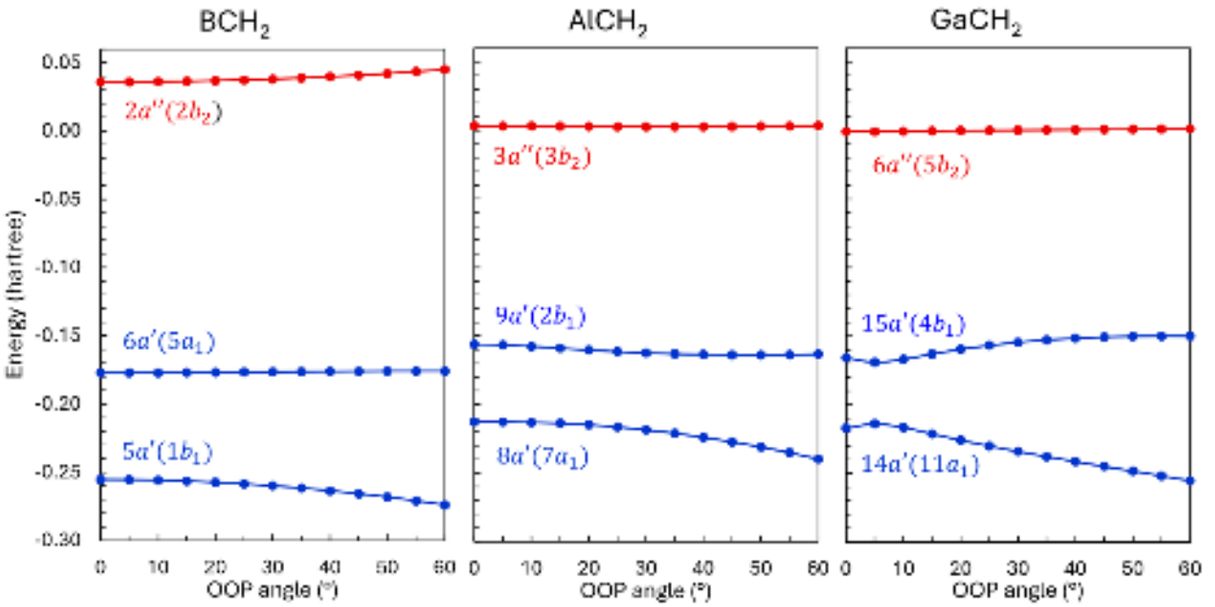

Figure 7: Variations in orbital energies (α electrons only) as a function of out-of-plane (OOP) angle for BCH_2, $AlCH_2$ and $GaCH_2$. The orbital energies were calculated at the CASSCF/aug-cc-pVTZ level of theory by changing the OOP angle while keeping all other geometric coordinates fixed at the equilibrium geometry of the ground state.

In $AlCH_2/GaCH_2$, the MO configurations, state symmetries and orbital energetics are just the opposite as shown in Fig. 7. The doubly occupied $7a_1$ orbital shows a lone pair directed away from the AlC/GaC bond whereas $2b_1$ is essentially an out-of-plane $2p$ orbital on the carbon atom, with little π bond character. On pyramidalization, the calculations indicate that $7a_1$ favors a low oop bending frequency, whereas the $2b_1$ energy is much less sensitive to oop bending. In the…$(7a_1)^2$ $(2b_1)^1$ ground state, the two electrons in the $7a_1$ MO result in ν_4'' = 445/404 cm^{-1} whereas the $7a_1 \rightarrow 2b_1$ electron promotion partially relieves the $7a_1$ influence, restoring ν_4' to a more usual value of 1 013/981 cm^{-1}.

VI. CONCLUSIONS

The major conclusion of this inquiry is that linear HBCH is the global minimum on the BCH_2 ground state potential energy surface and that the C_{2v} boron methylene radical isomer is 3 935 cm^{-1} higher in energy. The two are separated by an isomerization barrier of 12 825 cm^{-1} and the H_2BC isomer is a weakly bound species which easily reverts to the linear structure. These findings explain why HBCH has been detected in cryogenic matrices but BCH_2 has yet to be definitively observed spectroscopically.

The only viable electronic transition suitable for detecting BCH_2 by LIF or absorption spectroscopy is the $\tilde{C}^2B_2$ - $\tilde{X}^2A_1$ band system in the 320 - 290 nm region. This is at higher energy than a previous search we conducted for the BCH_2 spectrum, so if the radical was produced in our pulsed discharge source, we would not have detected it. The vibronic bands are predicted to have an open rotational structure suitable for detailed rotational analysis. The Franck-Condon profiles of the $\tilde{C} - \tilde{X}$ absorption bands and the allowed emission transitions $\tilde{C} - \tilde{X}$ and $\tilde{C} - \tilde{B}$ have been calculated for BCH_2 and BCD_2. Our calculations show that the lowest electronic transitions of the

HBCH free radical (bent−linear) occur in the near ultraviolet as well, adding an additional complication to an already difficult problem. The results of the present work should be useful in attempts to detect the boron methylene free radical by spectroscopic methods.

ACKNOWLEDGEMENTS

DJC thanks Tony C. Smith for his support and encouragement of the research and Fumie X. Sunahori for proofreading the manuscript. This work was funded by Ideal Vacuum Products.

AUTHOR DECLARATIONS

Conflict of interest

The authors have no conflicts to disclose.

DATA AVAILABILITY

The data that support the findings of this study are available within the article.

References

1. F. X. Sunahori, T. C. Smith and D. J. Clouthier, J. Chem. Phys. **157**, 044301 (2022).

2. T. C. Smith, R. Tarroni and D. J. Clouthier J. Chem. Phys. **160**, 024306 (2024).

3. R. Tarroni and D. J. Clouthier, J. Chem. Phys. **153**, 014301 (2020).

4. W. S. Rees, M. D. Hampton, S. W. Hall, J. L. Mills, P. Niedenzu, and S. G. Shore, Inorg. Synth. **27**, 339 (1990).

5. P. Hassanzadeh, Y. Hannachi and L. Andrews, J. Phys. Chem. **97**, 6418 (1993).

6. C. M. Cook and L. C. Allen, Organometallics, **1**, 246 (1982).

7. W. Fang and S. D. Peyerimhoff, Mol. Phys. **93**, 329 (1998).

8. Y. Zeng, K. Su, J. Deng, T. Wang, Q. Zeng, L. Cheng, and L. Zhang, Journal of Molecular Structure: THEOCHEM **861**, 103, (2008).

9. N. Jing, X. Zhang, J. Xu, and Y. Ding, Mol. Phys. **113**, 1271 (2015).

10. G. Mierzwa, A. Gordon, and S. Berski, Polyhedron **170**, 180 (2019).

11. Molpro, version 2010.1, a package of ab initio programs, H. -J. Werner, P. J. Knowles, and others, see https://www.molpro.net.

12. H.-J. Werner and P. J. Knowles, J. Chem. Phys. **82**, 5053 (1985)

13. P. J. Knowles and H.-J. Werner, Chem. Phys. Lett. **115**, 259 (1985).

14. H.-J. Werner and P. J. Knowles, J. Chem. Phys. **89**, 5803 (1988).

15. P. J. Knowles and H.-J. Werner, Chem. Phys. Lett. **145**, 514 (1988).

16 R. A. Kendall, T. H. Dunning, Jr, R. J. Harrison, J. Chem. Phys. **96**, 6796 (1992).

17. E. R. Davidson and D. W. Silver, Chem. Phys. Lett. **52**, 403 (1977).

18. H.-J. Werner, M. Kállay, and J. Gauss, J. Chem. Phys. **128**, 034305 (2008).

19. K. A. Peterson and T.H. Dunning, Jr., J. Chem. Phys. **117**, 10548 (2002).

20. D.-S. Yang, M. Z. Zgierski, A. Bérces, P. A. Hackett, P.-N. Roy, A. Martinez, T. Carrington, Jr., D. R. Salahub, R. Fournier, T. Pang, and C. Chen, J. Chem. Phys. **105**, 10663 (1996).

21. E. V. Doktorov, I. A. Malkin, and V. I. Man'ko, J. Mol. Spectrosc. **64**, 302 (1977).

22. PGOPHER, A Program for Simulating Rotational Structure, C. M. Western, University of Bristol, http://pgopher.chm.bris.ac.uk.

23. C. M. Western, J. Quant. Spectrosc. and Rad. Trans. **186**, 221 (2016).

24. K. R. Compaan, J. Agarwal, B. E. Dye, Y. Yamaguchi and H. F. Schaefer, III, Astrophys. J. **778**, 1, 2013.

25. M. A. Gharaibeh, D. J. Clouthier and R. Tarroni, J. Chem. Phys. **135**, 214307 (2011).

26. R. A. Grimminger, D. J. Clouthier and R. Tarroni, J. Chem. Phys. **135**, 214306 (2011).

27. L. S. Bartell and B. L. Carroll, J. Chem. Phys. **42**, 3076 (1965).

28. I. L. Alberts and H. F. Schaefer III, Chem. Phys. Lett. **165**, 250 (1990).

29. Z. Cao, J. Zhang, A. Tian and G. Yan, J. Mol. Struct. **333,** 181 (1995).

30. M. Michel, S. Kar, L. Endres, R. D. Dewhurst, B. Engels and H. Braunschweig, Nat. Syn. **4,** 869 (2025).

31. A. Batalov, J. Fulara, I. Shnitko and J. P. Maier, Chem. Phys. Lett. **404**, 315 (2005).

32. W. W. Harper, E. A. Ferrall, R. K. Hilliard, S. M. Stogner, R. S. Grev and D. J. Clouthier, J. Am. Chem. Soc. **119**, 8362 (1997).

33. H. Leclercq and I. Dubois, J. Mol. Spectrosc.**76**, 39 (1979).

34. W. W. Harper, K. Waddell and D. J. Clouthier, J. Chem. Phys., **107**, 8829 (1997).

35. D. A. Hostutler, T. C. Smith, H. Li and D. J. Clouthier, J. Chem. Phys., **111**, 950 (1999).

36. T. C. Smith, H. Li and D. J. Clouthier, J. Chem. Phys., **114**, 9012 (2001).

37. D. A. Hostutler, D. J. Clouthier, and S. W. Pauls, J. Chem. Phys., **116**, 1417 (2002).

38. T. C. Smith, C. J. Evans and D. J. Clouthier, J. Chem. Phys. **118**, 1642 (2003).

39. S.-G. He, B. S. Tackett and D. J. Clouthier, J. Chem. Phys. **121**, 257 (2004).

40. T. C. Smith, M. Gharaibeh and D. J. Clouthier, J. Chem. Phys. **157,** 204306 (2022).

41. D. J. Clouthier and D. A. Ramsay, Annu. Rev. Phys. Chem. **34**, 31 (1983).

42. R. J. Glinski, C. D. Taylor and H. R. Martin, J. Phys. Chem. **95,** 6159 (1991).